Journal of Biomechanics 43 (2010) 900–905

Contents lists available at ScienceDirect

Journal of Biomechanics

journal homepage: www.elsevier.com/locate/jbiomech
www.JBiomech.com

Cells in 3D matrices under interstitial flow: Effects of extracellular matrix alignment on cell shear stress and drag forces

John A. Pedersen [a], Seth Lichter [b], Melody A. Swartz [a,b,c,*]

[a] Department of Biomedical Engineering, Northwestern University, Evanston, IL 60208, USA
[b] Department of Mechanical Engineering, Northwestern University, Evanston, IL 60208, USA
[c] Institute of Bioengineering, École Polytechnique Fédérale de Lausanne (EPFL), SV - LMBM, Station 15, CH-1015 Lausanne, Switzerland

ARTICLE INFO

Article history:
Accepted 4 November 2009

Keywords:
Computational fluid dynamics
Mechanobiology
Perfusion
Collagen
Brinkman flow

ABSTRACT

Interstitial flow is an important regulator of various cell behaviors both *in vitro* and *in vivo*, yet the forces that fluid flow imposes on cells embedded in a 3D extracellular matrix (ECM), and the effects of matrix architecture on those forces, are not well understood. Here, we demonstrate how fiber alignment can affect the shear and pressure forces on the cell and ECM. Using computational fluid dynamics simulations, we show that while the solutions of the Brinkman equation accurately estimate the average fluid shear stress and the drag forces on a cell within a 3D fibrous medium, the distribution of shear stress on the cellular surface as well as the peak shear stresses remain intimately related to the pericellular fiber architecture and cannot be estimated using bulk-averaged properties. We demonstrate that perpendicular fiber alignment of the ECM yields lower shear stress and pressure forces on the cells and higher stresses on the ECM, leading to decreased permeability, while parallel fiber alignment leads to higher stresses on cells and increased permeability, as compared to a cubic lattice arrangement. The Spielman–Goren permeability relationships for fibrous media agreed well with CFD simulations of flow with explicitly considered fibers. These results suggest that the experimentally observed active remodeling of ECM fibers by fibroblasts under interstitial flow to a perpendicular alignment could serve to decrease the shear and drag forces on the cell.

1. Introduction

Matrix alignment is common in tissue remodeling and interstitial cells like fibroblasts can readily align their extracellular matrix (ECM) according to mechanical and molecular cues. *In vivo*, these cues are typically a combination of biochemical (e.g. inflammatory factors such as TGF-β) and mechanical signals (Orr et al., 2006; MacKenna et al., 2000; Ingber, 2006; Rhee and Grinnell, 2007; Chiquet et al., 2009; Davies, 2009; Fritton and Weinbaum, 2009; Hahn and Schwartz, 2009; Riddle and Donahue, 2009). Matrix fiber alignment is seen in healing wounds (Tomasek et al., 2002) and other inflammatory environments, where interstitial flow (IF) is increased due to capillary hyperpermeability and immune cell infiltration. While normal IF can be in the range of 0.1–1 μm/s (Chary and Jain, 1989; Dafni et al., 2002), increased IF in such inflammatory environments are evidenced by drastically increased lymph flow rates (Mullins and Hudgens, 1987; Matsumoto et al., 1990; He et al., 2002; Modi et al., 2007) because lymph drains the interstitial space. In addition to its role in wound healing, IF is important for tissue homeostasis via transport of metabolites and cell-signaling molecules; it is also an important morphoregulator both *in vivo* (Boardman and Swartz, 2003; Hirokawa et al., 2006; Schweickert et al., 2007) and *in vitro*, where it has been used to engineer functional blood and lymphatic capillaries (Ng et al., 2004; Helm et al., 2005; Semino et al., 2006; Helm et al., 2007).

The ways that cells perceive IF are poorly understood. The cells might directly sense the surface forces induced by flow, the drag and tethering forces that result from these surface forces on the ECM, or the effects may be more indirect. For example, recent work has shown that IF can alter the extracellular distribution of secreted chemokines or morphogens and thus direct cell migration or capillary morphogenesis (Helm et al., 2005; Fleury et al., 2006; Shields et al., 2007). Flow may also be focused on small portions of a porous space by larger tissue structures and have a strong effect on cells embedded in that space (Tada and Tarbell, 2000).

Collagen matrices can align in the direction of mechanical strain (Harris et al., 1981; Barocas and Tranquillo, 1997). In contrast, IF-induced cell-mediated matrix realignment is perpendicular to the direction of flow (Ng and Swartz, 2003; Ng

* Corresponding author at: Institute of Bioengineering, SV - LMBM, Station 15, Ecole Polytechnique Fédérale de Lausanne (EPFL), 1015 Lausanne, Switzerland. Tel.: +41 21 693 9686; fax: +41 21 693 9685.
E-mail address: melody.swartz@epfl.ch (M.A. Swartz).

0021-9290/$ - see front matter © 2009 Elsevier Ltd. All rights reserved.
doi:10.1016/j.jbiomech.2009.11.007

and Swartz, 2006), and this alignment correlates with myofibroblast differentiation and increased fibrotic potential (Ng et al., 2005). It is also well-known that a matrix made of perpendicularly aligned fibers should experience greater drag force than matrices parallel to the direction of flow (Happel and Brenner, 1965; Jackson and James, 1986). Therefore, we wondered whether local matrix alignment could be a mechanism of stress shielding by the cell and asked how the fiber alignment would affect stresses on a cell embedded within this matrix. We present here a computational fluid dynamics (CFD) study to evaluate the shear and pressure forces on cells in matrices with different fiber alignments and show that perpendicular matrix alignment shields the cell from fluid stresses by transferring these forces onto the matrix fibers. Thus, by altering local fiber geometry, cells can alter the details of their local mechanical environment, even if the fiber rearrangement does not alter the bulk tissue porosity.

2. Theory

Typical approaches for modeling flow through porous media use a single parameter to describe the flow resistance of the solid phase of the media rather than modeling the media explicitly as a two-phase material. The hydraulic permeability, K, was first described empirically by Darcy (Darcy, 1856) and later modified by Brinkman to allow for fluid velocity gradients and the satisfaction of no-slip boundary conditions (Brinkman, 1947). Brinkman's equation, with a few modest corrections, has been theoretically validated using the Navier–Stokes equation and ensemble averages of spherical and fibrous obstacles (Tam, 1969; Lundgren, 1972; Chernyakov, 1998).

Fibrous media constitute a distinct subclass of porous media because the solid phase can be very sparse and may be oriented spatially, unlike granular porous media. As a result, permeability relationships designed for particle suspensions, packed beds, and other non-fibrous media typically have a poor fit with experimental results on the permeability of fibrous media (Jackson and James, 1986). We previously found good correlation between the average shear stress on a sphere in a 3D fiber lattice computed by CFD and that predicted by the Brinkman equation, provided that the relationship used to compute the permeability (K) is appropriate for fibrous media (Pedersen et al., 2007); however, the shear distribution and the peak values of shear stress were not well predicted by the Brinkman equation using several published K relationships. While average stresses on cells in complex 3D structures can be well predicted using simpler models, knowledge of shear stress maxima and distributions on cells requires a 3D geometrical model (Boschetti et al., 2006), since the architecture of the matrix determines the gradients in shear stress. Here our goal is to determine the effects of local ECM fiber alignment on fluid forces on the cell. Thus, to compare our CFD results with analytical predictions, we consider previous continuum-based models that estimate K in aligned fibrous matrices.

Spielman and Goren presented permeability relationships for random and aligned fibrous matrices which have been substantiated by, or compare well with, later work by other groups (Spielman and Goren, 1968; Jackson and James, 1986; Higdon and Ford, 1996; Chernyakov, 1998). Their computations resulted in implicit relationships between a dimensionless permeability (K/r_f^2, where r_f is the fiber diameter) and the solid volume fraction of the medium, φ_s, for matrices with fibers aligned randomly, parallel to flow, or perpendicular to flow, respectively:

$$\frac{1}{3}+\frac{5}{6}\frac{\sqrt{K}}{r_f}\frac{K_1(r_f/\sqrt{K})}{K_0(r_f/\sqrt{K})}=\frac{1}{4\varphi_s} \tag{1}$$

$$\frac{1}{2}\frac{\sqrt{K}}{r_f}\frac{K_1(r_f/\sqrt{K})}{K_0(r_f/\sqrt{K})}=\frac{1}{4\varphi_s} \tag{2}$$

$$\frac{1}{2}+\frac{\sqrt{K}}{r_f}\frac{K_1(r_f/\sqrt{K})}{K_0(r_f/\sqrt{K})}=\frac{1}{4\varphi_s} \tag{3}$$

$K_p(x)$ is the modified Bessel function of the second kind with order p and argument x, and $\varphi_s<0.75$. Once K is known for a given matrix, whether via direct measurement in an experiment or by using a theoretical relationship like those above, the Brinkman equation can be used to estimate the average shear stress on the surface of the sphere, as well as the fluid drag on the sphere from a given average flow velocity U_0. Ganapathy's form of the shear stress on a sphere in a Brinkman medium is (Ganapathy, 1997):

$$\tau=\frac{3}{2}\frac{U_0\mu}{a}\sin\theta\left(1+\frac{1}{\sigma}\right) \tag{4}$$

where

$$\sigma=\sqrt{\frac{K}{a^2}\left(1+\frac{5}{2}\varphi_s\right)} \tag{5}$$

Note that σ is a dimensionless permeability that is normalized by the embedded sphere (cell) radius, a, rather than the fiber radius, r_f, as in Eqs. 1–3. μ is the fluid viscosity, and θ is the angle from the free stream velocity axis.

Using Ganapathy's notation, the total drag on a sphere in a Brinkman medium is

$$D=U_0a\mu\left[2\pi\left(1+\frac{1}{\sigma}+\frac{1}{\sigma^2}\right)+4\pi\left(1+\frac{1}{\sigma}\right)\right] \tag{6}$$

The first term is the drag arising from the pressure gradient acting on the sphere and the second term is the integrated shear stress on the sphere surface.

Eqs. 1–6 describe the continuum-averaged approximations to the fluid flow around a cell embedded in a 3D fibrous matrix. Again, we note that these equations are based on descriptions of the matrix architecture that rely on only a permeability and solid volume fraction. Thus, as comparisons to our CFD solutions, Eqs. 1–5 were used to compute the Brinkman shear stress on the cell, while Eqs. 5 and 6 were used to compute the expected drag force. The results of these computations are referred to as the "Brinkman prediction" throughout this report.

3. Methods

Methods used in this study were similar to those described previously (Pedersen et al., 2007). Briefly, a 3D model of the fluid flow domain was created using Rhinocerous (v2.0, Robert McNeel & Assoc; Seattle, WA), centered on a spherical cell of radius a (7.5 μm) embedded in a lattice of fibers with diameter d and spacing s (Fig. 1). The domain was sufficiently large such that increasing its size had no effect on the computed results. The 3D models were exported in ACIS format, loaded into Gambit (v2.2, Fluent Inc; Lebanon, NH), and meshed using triangular face meshes and tetrahedral/hybrid volume elements. The mesh interval varied by model, but a grid convergence study based on the method of Roache (Roache, 1997) showed that the meshes used were sufficiently fine that the shear stress results were not adversely affected by the grid spacing (data not shown).

Models were designed in sets of three to test the effects of fiber organization on the fluids forces on cells embedded in the matrices (Fig. 1 and Table 1). For instance, models A1, B1 and C1 all had fiber diameters of 500 nm and a porosity of 98.4%; in A1, the fibers were organized in a cubic lattice, and in each of the other two fibers were organized in a square lattice that was either perpendicular (B1) or parallel (C1) to the flow direction. All lattices were homogenous—for any given model, both d and s were constant throughout the domain. To simulate cell-mediated matrix remodeling by fiber reorganization and realignment, we kept fiber diameter and porosity (fluid volume fraction) constant and allowed fiber spacing to change.

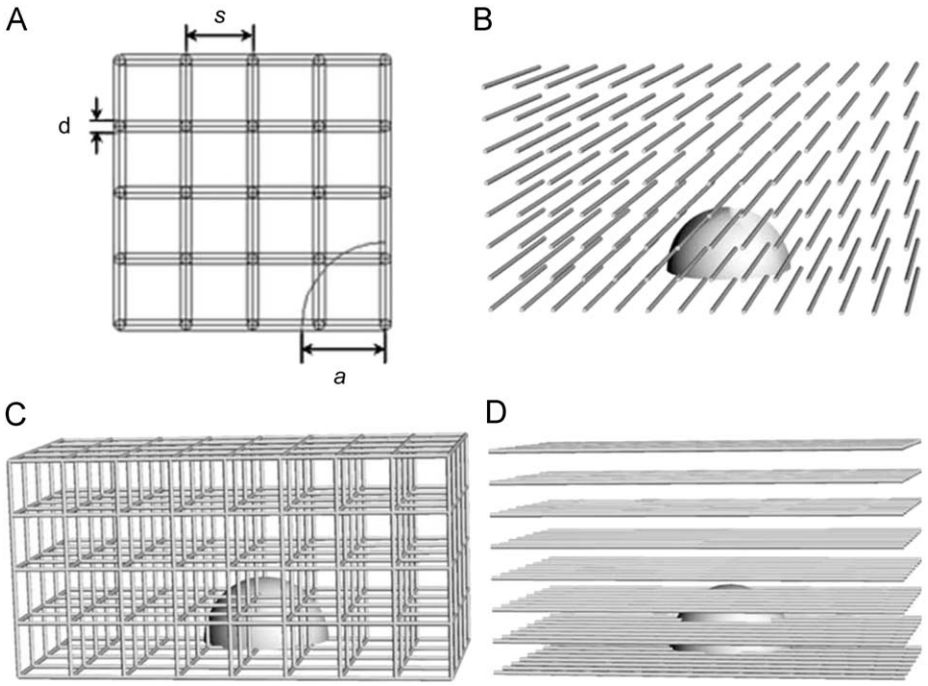

Fig. 1. CFD model setup. (A) Definition of the geometrical parameters of the model. Panels (B–D) show rendered samples of a cell in a matrix with fibers aligned perpendicular to flow (B), a cubic fiber lattice (C), and a matrix with fibers aligned parallel to flow (D). Flow is from left to right.

Table 1
Summary of computational model parameters.

	Alignment	d (nm)	s (μm)	K (μm^2)	ε
A1	Cubic	500	6.0	2.554	98.4%
B1	Perpendicular	500	3.5	1.595	98.4%
C1	Parallel	500	3.5	2.856	98.4%
A2	Cubic	700	4.0	0.737	93.4%
B2	Perpendicular	700	2.4	0.447	93.3%
C2	Parallel	700	2.4	0.828	93.3%
A3	Cubic	750	6.0	1.751	96.6%
B3	Perpendicular	750	3.6	1.222	96.6%
C3	Parallel	750	3.6	2.192	96.6%
D	Cubic	1000	6.0	1.356	94.0%

4. Results

In vivo, interstitial flow is driven by pressure gradients resulting from hydrostatic and osmotic pressure differences between the blood and the interstitial space (Guyton, 1963). When the ECM is remodeled in a way that changes K, the pressure gradient remains the same so the flow rate would vary; in this way, the effects of remodeling would be to change the local flow rates and distributions of flow through the matrix. Therefore we used fixed pressure gradients and found that for a given pressure drop, a cell embedded within idealized fibrous matrices experiences smaller shear stresses (both average and maximum) when the lattice is perpendicularly aligned as opposed to cubic, for the same porosity (Fig. 2). This was in contrast to the shear stresses on the ECM fibers, which were higher overall on a perpendicularly aligned matrix than on those aligned in a random or parallel direction, as expected (Spielman and Goren, 1968; Jackson and James, 1986). In addition, both the pressure and shear drag on the cell were lower in perpendicularly aligned (vs. cubic) matrices (Fig. 3 A,B).

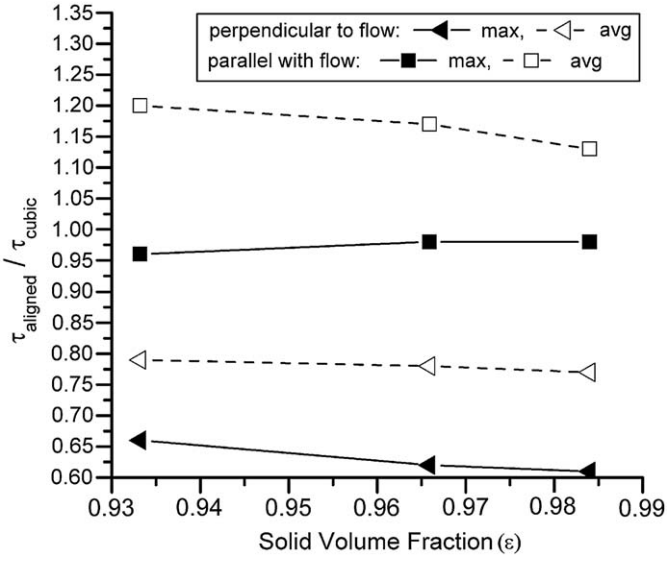

Fig. 2. Under a constant pressure gradient, cells in matrices aligned perpendicular to flow are subjected to lower maximum (solid) and average (dashed) shear stresses as compared to those in cubic lattices with the same fiber diameter and porosity. In contrast, cells in matrices aligned with flow experience nearly the same maximum shear stress as cells in cubic lattices, while average shear stress is elevated between 10% and 20% compared to the cubic lattice case.

In addition to total fluid forces, the distribution of shear stress on the cell surface was also significantly altered by fiber alignment. In a perpendicularly aligned matrix (e.g., model B2), there were more discrete areas of maximal shear stress distributed over a larger area than those in a cubic lattice (model A2). When fibers were aligned parallel to flow (model C2), there was a smoother shear stress distribution around the cell (Fig. 3A), but the average and integrated shear stresses, shear drag, and

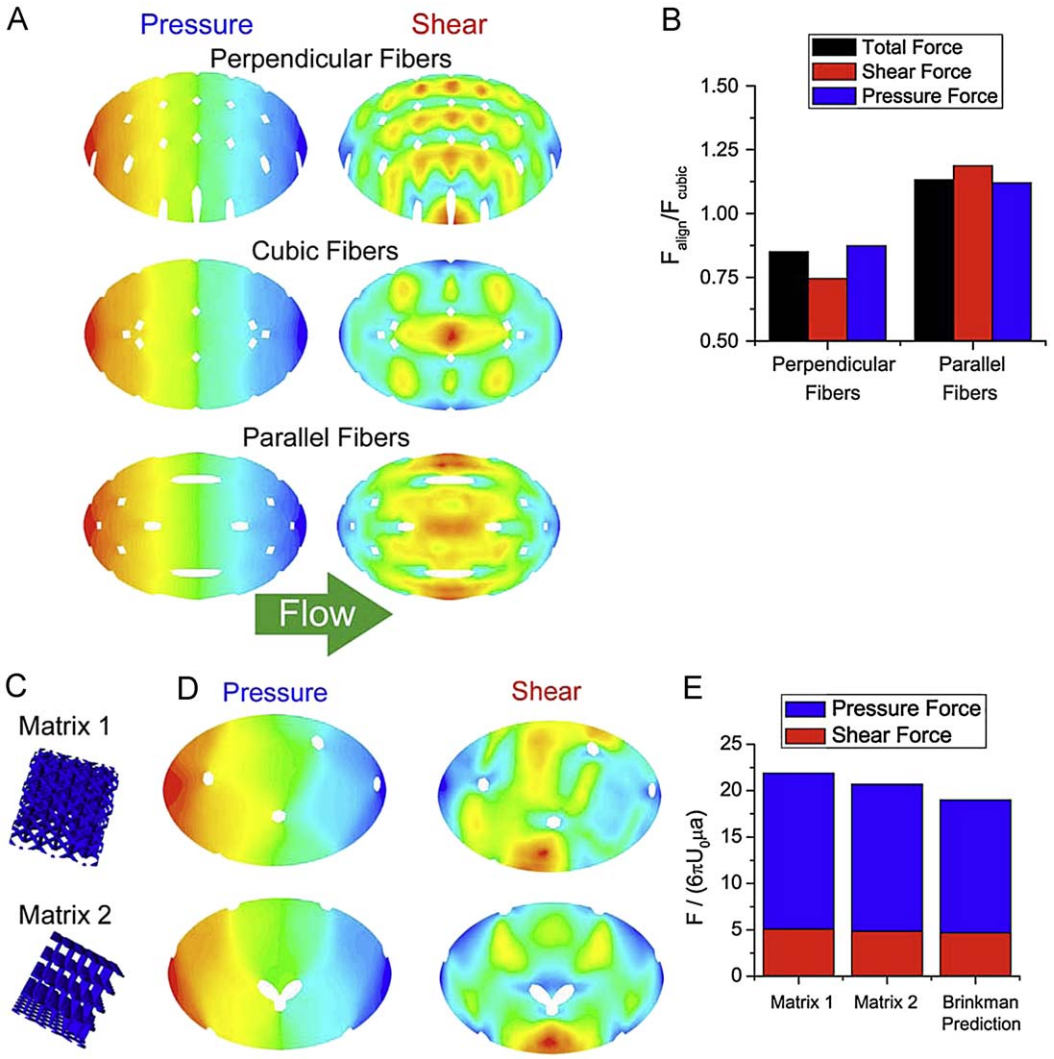

Fig. 3. For a fixed pressure gradient, remodeling the ECM (in such a way as to keep the porosity constant) from a cubic fiber architecture to one where the fibers are aligned perpendicular to flow shields the cell from both shear and pressure drag. Remodeling the ECM from a cubic fiber architecture to one where fibers are aligned parallel to flow, however, results in an increase in both pressure and shear drag. (A) Relative pressure and shear distributions on a quadrant of a cell undergoing flow through perpendicular, cubic, and parallel fiber matrices, respectively. Scale is from red (maximum) to blue (minimum), with white spaces showing where fibers intersect the cell surface. (B) Total or integrated forces on the entire cell surface relative to those in a cubic lattice. (C–E). Rotating a 3D cubic lattice (matrix D) with respect to the flow direction significantly changes the shear distribution on a cell embedded within it, but does not alter the pressure distribution. (C) Matrix 1 was rotated 45° in the *xy* and *xz* planes, while matrix 2 was rotated 45° in the *xy* plane only. (D) Relative pressure and shear distributions (red, maximum to blue, minimum). White spaces indicate fiber intersections with cell. (E) Integrated (total) dimensionless shear and pressure forces on the cell in each matrix compared with that predicted from Brinkman's equation.(For interpretation of the references to colour in this figure legend, the reader is referred to the web version of this article.)

pressure drag on the cell were higher than those found in models A2 or B2 (Fig. 3B).

Although the fiber size and matrix porosity were held constant between matrices, the effective K was different (Eqs. 1–3)—parallel alignment had a higher K than a cubic lattice, increasing the flow velocity, while perpendicular alignment had the lowest K, in turn decreasing the overall flow velocities. Thus, by remodeling its local matrix in a perpendicular alignment to interstitial flow, the cell reduces its shear stress and drag forces, and slows the local flow around it. We can expect from Darcy's Law that K^{-1} reflects the overall drag of the fibers (Spielman and Goren, 1968), and thus the drag on the matrix fibers in a perpendicularly aligned matrix is higher than that on fibers in the same matrix if it is aligned parallel to flow (Eqs. 2 and 3). Therefore, while the cell becomes shielded from fluid forces by remodeling its matrix to a perpendicular alignment, the matrix absorbs them.

Rotating a cubic fiber lattice should not affect its K because cubic lattices have no preferred direction. To ensure that the model results were not due to the co-alignment of the flow and fibers, models were constructed with the matrix rotated with respect to the flow direction. In Fig. 3 C–E, matrix D was rotated 45° in either two planes (matrix 1) or one plane (matrix 2). While rotating the cubic fiber lattice redistributed shear on the cell surface, average shear stresses for the two models were within 5% of each other and of Matrix D, and integrated pressure and drag forces were within 6%; these are near the expected error predicted by a grid convergence study (data not shown). Therefore, rotating the cubic lattice did not change the K or average shear stresses on the cell.

To compare with continuum-based approaches, we determined the permeability of our fibrous matrices by modeling the flow (without a cell in place) using constant velocity boundary conditions until it reached steady state, and then "measuring" the pressure drop required to drive that flow as determined by the simulation. Once the flow speed and pressure drop were known, we solved the Darcy equation for K and compared it to Spielman

and Goren's predictions for matrices with the same porosities. For cubic fiber lattices, our CFD permeabilities matched well with the Spielman and Goren predictions (Fig. 4). Therefore, our results for average fluid forces on the cell were consistent with results obtained from the Brinkman equation with Spielman and Goren's K.

Finally, examining the Brinkman equation for drag on a sphere in a porous matrix shows that the majority of the drag force on cells in typical *in vitro* fibrous matrices is from the pressure drag (Fig. 5, Eq. (6)). Using K as measured from the CFD simulations yields dimensionless permeability (σ) values between 0.1 and 0.2. Eq. (6) shows that in this range, pressure drag accounts for 72–85% of the total drag on the cell; our CFD results confirm this finding (see discussion below). Thus, as matrices become more restricted (as many *in vivo* matrices are), K decreases and the pressure forces become more dominant compared to shear forces. By contrast, in matrices with very high porosities (such as the sparse matrices often used for 3D *in vitro* experiments), the shear on the cell will account for a higher fraction of the drag and thus may be a stronger signal to the cell regarding the local flow environment.

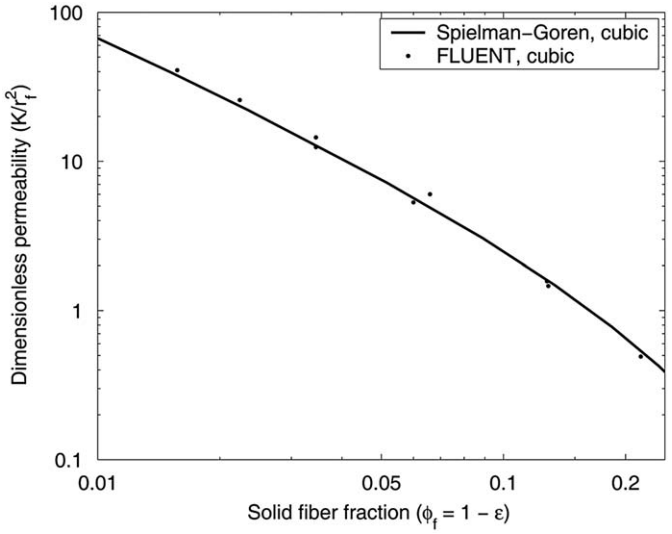

Fig. 4. K computed using Spielman and Goren's relationship (Eq. (1)) agrees well with K estimated by the CFD (FLUENT) simulations for a cubic lattice.

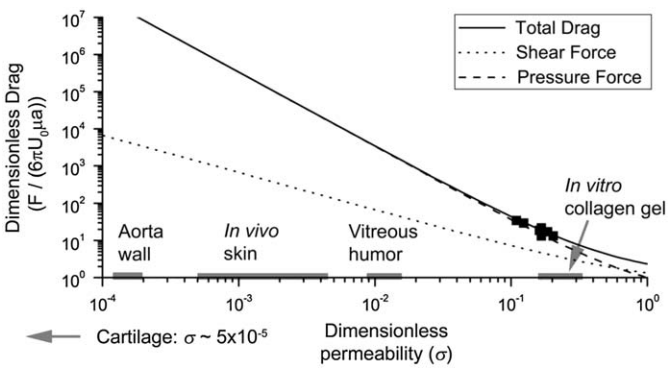

Fig. 5. Forces (normalized to Stokes' drag on a sphere) on a cell embedded in 3D fibrous matrices as a function of permeability reveal that pressure forces on the cell dominate as matrices become more dense and restrictive to flow.

5. Discussion

The organization and density of the fibers around cells embedded in a 3D matrix define the distribution of shear stress on the surface of those cells, and together with the pressure gradient determine the magnitude of the shear and drag on those cells as well. Consequently, changes in the matrix architecture alter the forces imposed on a cell by interstitial flow. Thus, by changing local ECM fiber organization, cells can modulate their mechanical environment.

Using CFD simulations, we demonstrated that the average, but not peak, shear stresses and pressure drag forces on a cell embedded in an *in vitro* fibrous matrix with no preferred orientation are accurately predicted using continuum approximations such as those calculated from Ganapathy's solution (Eqs. 4–6). Instead, the peak magnitudes and shear stress distributions on the cell surface depend on the details of the local fiber architecture, and are also significantly affected by the matrix alignment even more than would be predicted by computing a permeability that takes fiber alignment into account.

We have previously shown that the rearrangement of only a few fibers close to the cell can result in a mitigation of the shear stress on the cellular surface (Pedersen et al., 2007) without affecting K, but our results here show that the shear force might be a small part of the total drag on the cell. Furthermore, interstitial cells are capable of remodeling the architecture of the entire matrix given sufficient time (Grinnell and Lamke, 1984; Ng et al., 2005); thus, altering the global architecture will alter the matrix permeability thereby altering the pressure forces on the cells inside the matrix.

As the matrix becomes more restricted, pressure forces dominate the shear forces. For example, as computed in model A2, the pressure gradient required to drive flow at 4 μm/s was 4.3×10^{-3} Pa/μm; integrating this across the cell surface yields a pressure drag of 12.7 pN. Peak shear stress was 1.2×10^{-2} Pa, but the integrated shear drag was 2.8 pN. A similar pattern held for all models reported here.

Our estimate of the tethering forces required to hold a cell in place against the fluid forces directly imposed on the cell is very small compared to other cellular-scale forces. The drag on a cell in a typical matrix under 4 μm/s flow was about 16 pN (see discussion above). Assuming 10 fibers are placed under tension to hold the cell in place against this drag, the load on a single fiber/cell junction would be a mere 1.6 pN. By comparison, the bond-strength of a typical integrin–ligand interaction is 40 pN (Lehenkari and Horton, 1999; Sun et al., 2005), and fibroblasts appear to be capable of exerting 10 nN of force with a single focal adhesion on fibronectin (Tan et al., 2003). However, matrix tension from fluid drag on the matrix itself, which may in turn be transmitted to integrins, might be much larger than the direct effect on the cell. For example, the fibers in the model A2 domain absorb approximately 470 pN of drag (computed from the pressure drop across the domain). If a significant percentage of this force is transmitted to the cell, it could overwhelm the direct drag on the cell computed above. The details of the force transmission will depend on how the matrix is organized and cross-linked (Pedersen and Swartz, 2005; Chandran and Barocas, 2006).

In conclusion, we have shown that fiber alignment determines the distribution and magnitude of peak forces on cells in the 3D interstitial space. We provide estimates for the magnitude of shear and pressure forces directly imposed on the cell by interstitial flow. Finally, we speculate based on these results that fluid forces and local fiber remodeling may interact to provide the cells with sensitive mechanical feedback as to the local and global state of the ECM matrix.

Conflict of interest statement

The authors have no conflicts of interest.

Acknowledgments

The authors are grateful to Mark Johnson and Matthew Glucksberg for helpful advice. This work was funded by the National Science Foundation (BES-0134551), the Whitaker Foundation (R-01-0348), and the Swiss National Science Foundation (107602).

References

Barocas, V.H., Tranquillo, R.T., 1997. An anisotropic biphasic theory of tissue-equivalent mechanics: the interplay among cell traction, fibrillar network deformation, fibril alignment, and cell contact guidance. Journal of Biomechanical Engineering 119, 137–145.

Boardman, K.C., Swartz, M.A., 2003. Interstitial fluid flow as a guide for lymphangiogenesis. Circulation Research 92, 801–808.

Boschetti, F., Raimondi, M.T., Migliavacca, F., Dubini, G., 2006. Prediction of the micro fluid dynamic environment imposed to three-dimensional engineered cell systems in bioreactors. Journal of Biomechanics 39, 418–425.

Brinkman, H.C., 1947. A calculation of the viscous force exerted by a flowing fluid on a dense swarm of particles. Applied Scientific Research A1, 27–34.

Chandran, P.L., Barocas, V.H., 2006. Affine vs. non-affine fibril kinematics in collagen networks: theoretical studies of network behavior. Journal of Biomechanical Engineering 128, 259–270.

Chary, S.R., Jain, R.K., 1989. Direct measurement of interstitial convection and diffusion of albumin in normal and neoplastic tissues by fluroescence photobleaching. Proceedings of the National Academy of Sciences of the United States of America 86, 5385–5389.

Chernyakov, A.L., 1998. Fluid flow through three-dimensional fibrous porous media. Journal of Experimental and Theoretical Physics 86, 1156–1165.

Chiquet, M., Gelman, L., Lutz, R., Maier, S., 2009. From mechanotransduction to extracellular matrix gene expression in fibroblasts. Biochimica Et Biophysica Acta—Molecular Cell Research 1793, 911–920.

Dafni, H., Israely, T., Bhujwalla, Z.M., Benjamin, L.E., Neeman, M., 2002. Overexpression of vascular endothelial growth factor 165 drives peritumor interstitial convection and induces lymphatic drain: Magnetic resonance imaging, confocal microscopy, and histological tracking of triple-labeled albumin. Cancer Research 62, 6731–6739.

Darcy, H.P.G., 1856. Détermination des lois d'écoulement de l'eau à travers le sable. Fontaines publiques de la ville de Dijon.

Davies, P.F., 2009. Hemodynamic shear stress and the endothelium in cardiovascular pathophysiology. Nature Clinical Practice Cardiovascular Medicine 6, 16–26.

Fleury, M.E., Boardman, K.C., Swartz, M.A., 2006. Autologous morphogen gradients by subtle interstitial flow and matrix interactions. Biophysical Journal 91, 113–121.

Fritton, S.P., Weinbaum, S., 2009. Fluid and Solute Transport in Bone. Flow-Induced Mechanotransduction. Annual Review of Fluid Mechanics 41, 347–374.

Ganapathy, R., 1997. Creeping flow past a solid sphere in a porous medium. Zeitschrift für Angewandte Mathematik und Mechanik 77, 871–875.

Grinnell, F., Lamke, C.R., 1984. Reorganization of hydrated collagen lattices by human skin fibroblasts. Journal of Cell Science 66, 51–63.

Guyton, A.C., 1963. A concept of negative interstitial pressure based on pressures in implanted perforated capsules. Circulation Research 12, 399–414.

Hahn, C., Schwartz, M.A., 2009. Mechanotransduction in vascular physiology and atherogenesis. Nature Reviews Molecular Cell Biology 10, 53–62.

Happel, J., Brenner, H., 1965. In: Low Reynolds Number Hydrodynamics.. Prentice-Hall, Inc., Englewood Cliffs, N.J.

Harris, A.K., Stopak, D., Wild, P., 1981. Fibroblast traction as a mechanism for collagen morphogenesis. Nature 290, 249–251.

He, C., Young, A.J., West, C.A., Su, M., Konerding, M.A., Mentzer, S.J., 2002. Stimulation of regional lymphatic and blood flow by epicutaneous oxazolone. Journal of Applied Physiology 93, 966–973.

Helm, C.-L.E., Fleury, M.E., Zisch, A.H., Boschetti, F., Swartz, M.A., 2005. 3D fluid flow directs capillary morphogenesis via biased amplification of VEGF gradients. Proceedings of the National Academy of Sciences of the United States of America 102, 15779–15784.

Helm, C.-L.E., Zisch, A.H., Swartz, M.A., 2007. Engineered blood and lymphatic capillaries in 3-D VEGF-fibrin-collagen matrices with interstitial flow. Biotechnology and Bioengineering 96, 167–176.

Higdon, J.J.L., Ford, G.D., 1996. Permeability of three-dimensional models of fibrous porous media. Journal of Fluid Mechanics 308, 341–361.

Hirokawa, N., Tanaka, Y., Okada, Y., Takeda, S., 2006. Nodal flow and the generation of left-right asymmetry. Cell 125, 33–45.

Ingber, D.E., 2006. Cellular mechanotransduction: putting all the pieces together again. FASEB Journal 20, 811–827.

Jackson, G.W., James, D.F., 1986. The permeability of fibrous porous media. Canadian Journal of Chemical Engineering 64, 364–374.

Lehenkari, P.P., Horton, M.A., 1999. Single integrin molecule adhesion forces in intact cells measured by atomic force microscopy. Biochemical and Biophysical Research Communications 259, 645–650.

Lundgren, T.S., 1972. Slow flow through stationary random beds and suspensions of spheres. Journal of Fluid Mechanics 51, 273–299.

MacKenna, D.A., Summerour, S.R., Villarreal, F.J., 2000. Role of mechanical factors in modulating cardiac fibroblast function and extracellular matrix synthesis. Cardiovascular Research 46, 257–263.

Matsumoto, N., Koike, K., Yamada, S., Staub, N.C., 1990. Caudal mediastinal node lymph flow in sheep after histamine or endotoxin infusions. American Journal of Physiology 258, H24–H28.

Modi, S., Stanton, A.W., Mortimer, P.S., Levick, J.R., 2007. Clinical assessment of human lymph flow using removal rate constants of interstitial macromolecules: a critical review of lymphoscintigraphy. Lymphatic Research and Biology 5, 183–202.

Mullins, R.J., Hudgens, R.W., 1987. Increased skin lymph protein clearance after a 6-h arterial bradykinin infusion. American Journal of Physiology 253, H1462–H1469.

Ng, C.P., Swartz, M.A., 2003. Fibroblast alignment under interstitial fluid flow using a novel 3-D tissue culture model. American Journal of Physiology: Heart and Circulatory Physiology 284, H1771–H1777.

Ng, C.P., Helm, C.-L.E., Swartz, M.A., 2004. Interstitial flow differentially stimulates blood and lymphatic endothelial cell morphogenesis in vitro. Microvascular Research 68, 258–264.

Ng, C.P., Hinz, B., Swartz, M.A., 2005. Interstitial flow movement is sufficient to induce a fibrotic response in fibroblasts in vitro. Journal of Cell Science 118, 4731–4739.

Ng, C.P., Swartz, M.A., 2006. Mechanisms of interstitial flow-induced remodeling of fibroblast-collagen cultures. Annals of Biomedical Engineering 34, 446–454.

Orr, A.W., Helmke, B.P., Blackman, B.R., Schwartz, M.A., 2006. Mechanisms of mechanotransduction. Developmental Cell 10, 11–20.

Pedersen, J.A., Swartz, M.A., 2005. Mechanobiology in the 3rd dimension. Annals of Biomedical Engineering 33, 1469–1490.

Pedersen, J.A., Boschetti, F., Swartz, M.A., 2007. Effects of extracellular fiber architecture on cell membrane shear stress in a 3D fibrous matrix. Journal of Biomechanics 40, 1484–1492.

Rhee, S., Grinnell, F., 2007. Fibroblast mechanics in 3D collagen matrices. Advanced Drug Delivery Reviews 59, 1299–1305.

Riddle, R.C., Donahue, H.J., 2009. From Streaming Potentials to Shear Stress: 25 Years of Bone Cell Mechanotransduction. Journal of Orthopaedic Research 27, 143–149.

Roache, P.J., 1997. Quantification of uncertainty in computational fluid dynamics. Annual Review of Fluid Mechanics 29, 123–160.

Schweickert, A., Weber, T., Beyer, T., Vick, P., Bogusch, S., Feistel, K., Blum, M., 2007. Cilia-driven leftward flow determines laterality in Xenopus. Current Biology 17, 60–66.

Semino, C.E., Kamm, R.D., Lauffenburger, D.A., 2006. Autocrine EGF receptor activation mediates endothelial cell migration and vascular morphogenesis induced by VEGF under interstitial flow. Experimental Cell Research 312, 289–298.

Shields, J.D., Fleury, M.E., Yong, C., Tomei, A.A., Randolph, G.J., Swartz, M.A., 2007. Autologous chemotaxis as a mechanism of tumor cell homing to lymphatics via interstitial flow and autocrine CCR7 signaling. Cancer Cells 11, 526–538.

Spielman, L.A., Goren, S.L., 1968. Model for predicting pressure drop and filtration efficiency in fibrous media. Environmental Science and Technology 2, 279–287.

Sun, Z., Martinez-Lemus, L.A., Trache, A., Trzeciakowski, J.P., Davis, G.E., Pohl, U., Meininger, G.A., 2005. Mechanical properties of the interaction between fibronectin and $\alpha_5\beta_1$-integrin on vascular smooth muscle cells studied using atomic force microscopy. American Journal of Physiology-Heart and Circulatory Physiology 289, H2526–H2535.

Tada, S., Tarbell, J.M., 2000. Interstitial flow through the internal elastic lamina affects shear stress on arterial smooth muscle cells. American Journal of Physiology: Heart and Circulatory Physiology 278, H1589–H1597.

Tam, C.K.W., 1969. The drag on a cloud of spherical particles in low Reynolds number flow. Journal of Fluid Mechanics 38, 537–546.

Tan, J.L., Tien, J., Pirone, D.M., Gray, D.S., Bhadriraju, K., Chen, C.S., 2003. Cells lying on a bed of microneedles: An approach to isolate mechanical force. Proceedings of the National Academy of Sciences of the United States of America 100, 1484–1489.

Tomasek, J.J., Gabbiani, G., Hinz, B., Chaponnier, C., Brown, R.A., 2002. Myofibroblasts and mechanoregulation of connective tissue remodeling. Nature Reviews: Molecular Cell Biology 3, 349–363.